





The microRNAs miR-302b and miR-372 regulate mitochondrial metabolism via the SLC25A12 transporter, which controls MAVS-mediated antiviral innate immunity

Received for publication, August 5, 2019, and in revised form, November 20, 2019. Published, Papers in Press, November 25, 2019, DOI 10.1074/jbc.RA119.010511

Kai Yasukawa^{‡§}, Daisuke Kinoshita[‡], Keisuke Yaku[¶],  Takashi Nakagawa^{¶||}, and  Takumi Koshiba^{‡**1}

From the [‡]Department of Biology, Faculty of Science, Kyushu University, Fukuoka 819-0395, Japan, the [§]Modality Laboratories, Innovative Research Division, Mitsubishi Tanabe Pharma Corp., Fujisawa 251-8555, Japan, the [¶]Department of Metabolism and Nutrition, Graduate School of Medicine and Pharmaceutical Science for Research, and ^{||}Frontier Research Core for Life Science, University of Toyama, Toyama 930-0194, Japan, and the ^{**}Department of Chemistry, Faculty of Science, Fukuoka University, Fukuoka 814-0180, Japan

Edited by Craig E. Cameron

MicroRNAs (miRNAs) are small noncoding RNAs that suppress the expression of multiple genes and are involved in numerous biologic functions and disorders, including human diseases. Here, we report that two miRNAs, miR-302b and miR-372, target mitochondrial-mediated antiviral innate immunity by regulating mitochondrial dynamics and metabolic demand. Using human cell lines transfected with the synthetic analog of viral dsRNA, poly(I-C), or challenged with Sendai virus, we found that both miRNAs are up-regulated in the cells late after viral infection and ultimately terminate the production of type I interferons and inflammatory cytokines. We found that miR-302b and miR-372 are involved in dynamin-related protein 1 (DRP1)-dependent mitochondrial fragmentation and disrupt mitochondrial metabolism by attenuating solute carrier family 25 member 12 (SLC25A12), a member of the SLC25 family. Neutralizing the effects of the two miRNAs through specific inhibitors re-established the mitochondrial dynamics and the antiviral responses. We found that SLC25A12 contributes to regulating the antiviral response by inducing mitochondrial-related metabolite changes in the organelle. Structure–function analysis indicated that SLC25A12, as part of a prohibitin complex, associates with the mitochondrial antiviral-signaling protein in mitochondria, providing structural insight into the regulation of the mitochondrial-mediated antiviral response. Our results contribute to the understanding of how miRNAs modulate the innate immune response by altering mitochondrial dynamics and metabolic demand. Manipulating the activities of miR-302b and miR-372 may be a potential therapeutic approach to target RNA viruses.

MicroRNAs (miRNAs)² are short noncoding RNAs (~22 nucleotides) that act to suppress multiple genes widely

This work was supported by JSPS KAKENHI Grants 17H03667, 17K19561, and 18H04863, the Takeda Science Foundation, and the KANEKA Corp. (to T. K.). Kai Yasukawa is affiliated with Mitsubishi Tanabe Pharma Corp.

GEO accession number for the microarray data reported in this paper is GSE129615.

This article contains Figs. S1–S4 and Table S1.

¹ To whom correspondence should be addressed: Dept. of Chemistry, Faculty of Science, Fukuoka University, 8-19-1 Nanakuma, Jonan-ku, Fukuoka 814-0180, Japan. Tel.: 81-92-871-6631 (Ext. 6242); Fax: 81-92-865-6030; E-mail: koshiba@kyudai.jp.

² The abbreviations used are: miRNA or miR, microRNA; IFN- β , interferon β ; TNF- α , tumor necrosis factor α ; RANTES, regulated on activation normal T-cell expressed and secreted; RLR, retinoic acid-inducible gene I (RIG-I)-

expressed in eukaryotes, and they are linked to numerous biologic functions such as cell proliferation, differentiation, development, and apoptosis (1, 2). A primary mechanistic action of miRNA is that it interferes with mRNA, followed by imperfect annealing with each 3'-UTR of the target genes via their seed sequences that acts to repress translation and/or degradation results in gene silencing (1). To date, more than a thousand miRNAs have been identified in the human genome, many of which are implicated in human diseases (3). Recent studies revealed that several miRNAs also contribute to antiviral innate immunity (4–6).

In mammals, innate immunity against viral infection requires the activation of multiple signaling steps that culminate in the rapid production of type I interferons (IFN- α and - β) and other proinflammatory cytokines, such as tumor necrosis factor α (TNF α) and regulated on activation normal T-cell expressed and secreted (RANTES, also known as CCL5), that provide first-line host defense. The immune response is triggered by the recognition of broadly-conserved viral components, known as pathogen-associated molecular patterns (e.g. dsRNA or 5'-triphosphated single-stranded RNA), by host-encoded pattern recognition receptors (PRRs), and Toll-like receptor 3 and retinoic acid-inducible gene I (RIG-I)-like receptors (RLRs) act as the PRRs (7, 8). Especially in the RLR-mediated signal transduction pathway, the mitochondrion (the central powerhouse of eukaryotes) provides a molecular platform for facilitating the signaling event through MAVS, a downstream adaptor of RLRs located at the mitochondrial outer membrane (MOM) (9, 10). Although MAVS has a key role in signal transduction by recruiting various types of effectors at the MOM to orchestrate the “MAVS signalosome,” our previous studies demonstrated that fundamental functions of the

like receptor; MAVS, mitochondrial antiviral signaling protein; MOM, mitochondrial outer membrane; poly(I-C), polyinosinic–polycytidylic acid; SeV, Sendai virus; qPCR, quantitative PCR; HAU, hemagglutinin units; p.i., post-infection; HEK293, human embryonic kidney 293; IRF-3, interferon regulatory factor 3; MIM, mitochondrial inner membrane; PHB, prohibitin; IMS, mitochondrial intermembrane space; OCR, oxygen consumption rate; BRET, bioluminescence resonance energy transfer; FCCP, carbonyl cyanide-*p*-trifluoromethoxyphenylhydrazone; Ab, antibody; pAb, polyclonal antibody; PRR, pattern recognition receptor; ELISA, enzyme-linked immunosorbent assay.

mitochondria, including the mitochondrial membrane potential (11, 12), activity of oxidative phosphorylation (13), and mitochondrial dynamics (11, 14), are involved in mitochondrial (MAVS)-mediated innate immunity.

In this study, we investigated the mechanistic and functional roles of miRNAs in mitochondrial-mediated innate immunity. Although some miRNAs were previously demonstrated to be involved in antiviral innate immunity (4–6, 15), how those miRNAs function to facilitate innate immunity by changing the mitochondrial potentials has remained unclear. We clarified that two miRNAs, miR-302b and miR-372, which are involved in the embryonic stem cell–specific cell cycle and cell reprogramming (16, 17), target mitochondrial-mediated antiviral innate immunity through their regulation of mitochondrial dynamics and metabolic demand. These insights contribute to elucidate the mechanistic roles of the miRNAs essential for mitochondrial-mediated innate immunity, and manipulating these activities may be a potential therapeutic antiviral target.

Results

Searching for microRNAs linked to antiviral innate immunity and mitochondrial dynamics

To elucidate the expression profile of miRNAs in cells that respond to a viral infection event, we first evaluated changes in miRNA expression in human embryonic kidney 293 (HEK293) cells, a widely-used human cell line that responds to a synthetic analog of viral dsRNA, poly(I-C) transfection. We followed 53 miRNAs that were up-regulated more than 3-fold in poly(I-C)-transfected cells relative to those in the mock state (Table S1). To confirm that we would be observing a specific response to activation of the RLR-dependent signaling pathway, we induced another viral infection using Sendai virus (SeV), a negative-stranded RNA virus of the Paramyxoviridae family. Remarkably, nine miRNA candidates (miR-1250, miR-143, miR-302b, miR-338, miR-372, miR-410, miR-485, miR-520f, and miR-922) were well-matched between these two different stimuli (Fig. 1A and Table S1).

We therefore evaluated whether these miRNAs with increased levels had a role in the RLR-signaling pathway. Although the delivery of poly(I-C) into HEK293 cells potently activated an IFN- β luciferase-based reporter (Fig. 1B, NC), co-transfection of each miRNA mimic with poly(I-C) had various effects on the activation of its reporter. Among the nine candidates mentioned above, we confirmed that the delivery of three miRNA mimics (miR-302b, miR-372, and miR-520f) with poly(I-C) was sufficient to inhibit signal transduction (Fig. 1B). Interestingly, the delivery of two miRNA mimics, miR-302b and miR-372, in HeLa cells (widely used for mitochondrial imaging) led to extensively fragmented mitochondria (Fig. 1C and Table 1). These findings suggest that miR-302b and miR-372 affected the activity of both the RLR pathway and mitochondrial morphology. Because miR-302b and miR-372 have homologous seed sequences that can target overlapping genes (18), we mainly analyzed the function of miR-302b and confirmed the results against miR-372 in the following experiments.

miR-302b acts as a negative regulator of the mitochondrial-mediated antiviral response

Having identified that miR-302b (also miR-372) might link antiviral cellular innate immunity with mitochondrial potentials, we evaluated the functional role of the miRNA involved in mitochondrial-mediated antiviral innate immunity. The kinetic profile of IFN- β expression in A549 cells (widely used in viral research) infected with SeV peaked at 6 h post-infection (p.i.) as detected by quantitative PCR (qPCR), and the IFN- β mRNA level was sharply decreased at 12 h p.i. (Fig. 1D, top), which is a typical antiviral immune response (19). Expression of miR-302b, which was delayed relative to that of IFN- β , was induced 12 h after infection and increased for up to 36 h p.i.; this lagging trend in the expression was also observed in cells transfected with poly(I-C) (Fig. 1D, bottom; see also Fig. S1A). To verify that the observed RLR-mediated up-regulation of miR-302b was not due to a specific characteristic of the cell type we used, we performed the same miRNA induction experiments in other human cell lines, MRC-5 (fetal lung fibroblasts) and HAP-1 (widely used for biomedical and genetic research), and confirmed that both cell types also exhibited increased expression of miR-302b (Fig. 1E and Fig. S1B).

Because altering the level of miR-302b in cells would be consistent with an antiviral immune response (Fig. 1, B and D), we hypothesized that the miRNA acts as a modulator of the RLR-signaling pathway. To test this hypothesis, we treated HEK293 cells with the miR-302b mimic and assessed their immune response against either viral infection or poly(I-C) stimulation. The viral-triggered induction of IFN- β and other pro-inflammatory cytokines such as RANTES or TNF α was dramatically suppressed in cells transfected with the miR-302b mimic (Fig. 1F and Fig. S1, C and D). In addition, we confirmed that an abundant presence of the miR-302b mimic in the cells similarly attenuated the phosphorylation of endogenous interferon regulatory factor 3 (IRF-3; Fig. 1G), a hallmark of IRF-3 activation, and the production of endogenous IFN- β protein (Fig. 1H and Fig. S1, E and F). Treatment of HEK293 cells with the miR-302b mimic similarly reduced the activation of both IFN- β and NF- κ B reporters in response to overexpression of either the N-terminal CARD domain of RIG-I (designated as RIG-I^{1–250}) or MAVS, the MOM protein that acts downstream of RIG-I (Fig. S1G) (9). Most importantly, interfering with either endogenous miR-302b or miR-372 by applying its specific inhibitors to poly(I-C)-stimulated HEK293 (Fig. 2A) or HAP-1 (Fig. 2B) cells sufficiently increased the production of IFN- β . Taken together, these observations indicated that miR-302b (also miR-372) acts as a negative regulator of the mitochondrial-mediated antiviral response and suggests that it would act in the late stage of viral infection.

miR-302b regulates the DRP1-dependent pathway in the mitochondrial fission process

Because the accumulation of miR-302b in HeLa cells leads to remarkable mitochondrial fragmentation that is restored by the presence of its specific inhibitors (Fig. 3, A and B, and Fig. S2, A and B), we next attempted to elucidate whether certain molecules involved in mitochondrial dynamics are associated with

MicroRNAs regulate mitochondrial-mediated antiviral response

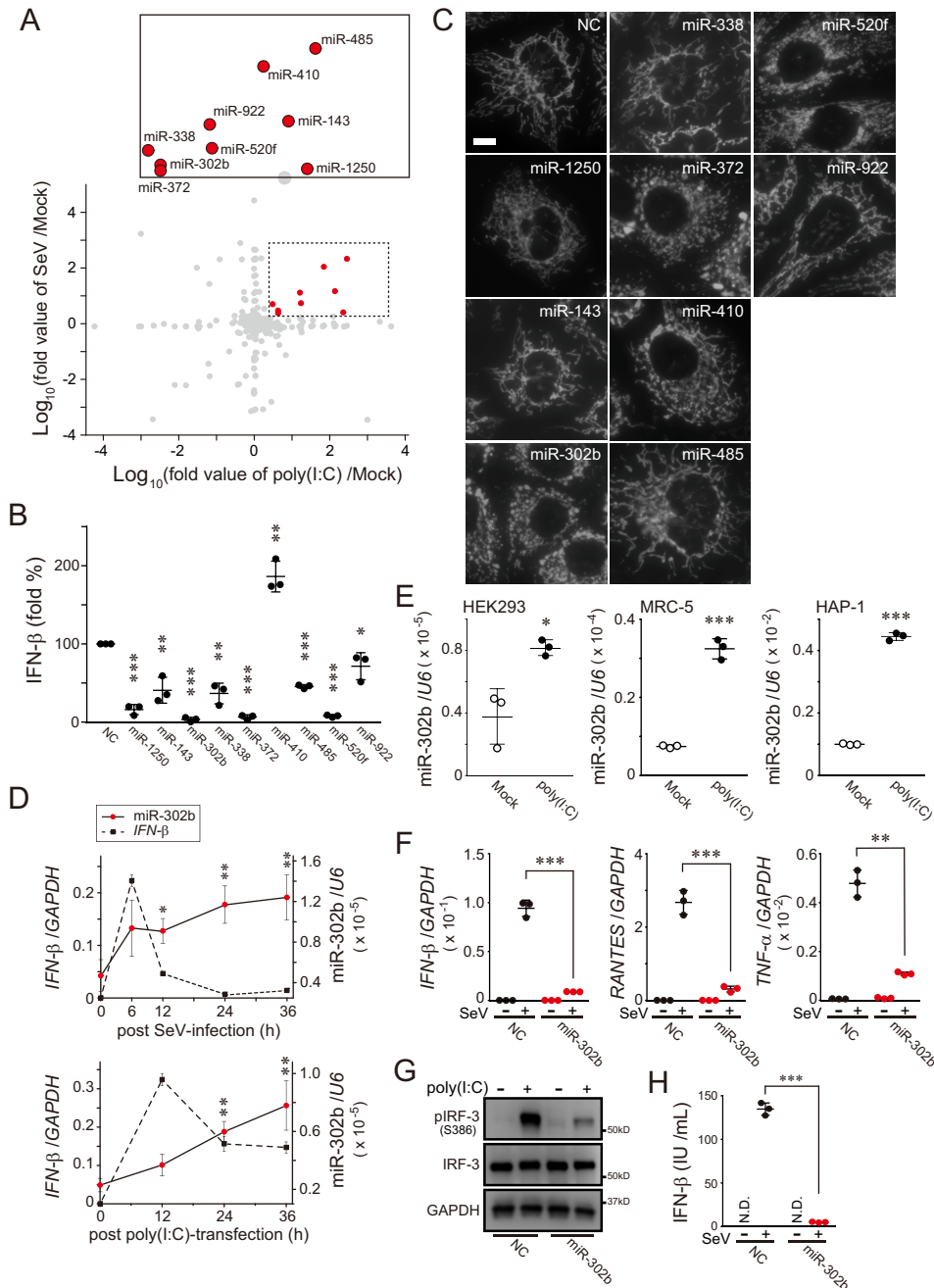


Figure 1. MicroRNAs that respond to RLR-mediated antiviral signaling. *A*, log-log plot showing fold-change in miRNA expression (analyzed by TaqMan low-density array) in HEK293 cells transfected with poly(I:C) (10 μ g for 24 h) versus Mock-transfected cells plotted against those of SeV infection (16 hemagglutinin units (HAU)/ml for 24 h) ($n = 1$). The dashed box in the graph shows the significantly increased miRNA area (abundance ratio > 2), and the inset on the top shows the annotated miRNAs from the dashed box. *B*, activation of the IFN- β reporter (p125luc) in miRNA mimic-treated HEK293 cells (each, 10 nM concentration) transfected with 500 ng of poly(I:C) for 24 h. NC (left in the graph) means negative control mimic. Data shown represent mean values \pm S.D. ($n = 3$). *, $p < 0.05$; **, $p < 0.01$, and ***, $p < 0.001$. *C*, indicated nine miRNA mimics were transfected in HeLa cells, and mitochondria in the cells were identified by stable expression of mitochondrially-targeted red fluorescent protein (12) by fluorescence microscopy. Scale bar, 10 μ m. NC, negative control mimic. *D*, kinetics of IFN- β and miR-302b expression in A549 cells with either SeV infection (top) or poly(I:C) transfection (bottom). The stimulated cells were collected at the indicated time points (0, 6, 12, 24, and 36 h) and analyzed by qPCR. Both GAPDH and U6 were used as internal controls. Data shown represent mean values \pm S.D. ($n = 3$). *, $p < 0.05$, and **, $p < 0.01$. *E*, expression profiles of miR-302b detected by qPCR in three cell lines (HEK293, MRC-5, and HAP-1) post-transfection with 5 μ g of poly(I:C) 24 h later. U6 was used as an internal control. Data shown represent mean values \pm S.D. ($n = 3$). *, $p < 0.05$; ***, $p < 0.001$. *F*, negative control or miR-302b mimic-transfected HEK293 cells were infected with SeV (4 HAU/ml) for 24 h, and the total RNAs from the cells were analyzed by qPCR for the expression of IFN- β , RANTES, TNF α , and GAPDH (internal control). Data shown represent mean values \pm S.D. ($n = 3$). **, $p < 0.01$ and ***, $p < 0.001$. *G*, similar to *F*, except that the cells were stimulated with 2 μ g of poly(I:C), and endogenous IRF-3 activation (phosphorylation) was detected by Western blotting. *H*, similar to *F*, except that the culture supernatants from cells were analyzed by ELISA to measure IFN- β production. N.D., not detected. Data shown represent mean values \pm S.D. ($n = 3$). ***, $p < 0.001$.

the phenomenon. To reveal its mechanistic actions, we performed microarray analysis in HEK293 cells transfected with the miR-302b mimic. Gene expression profiling of the cells

revealed an association of miR-302b with the mitochondrial dynamics (Fig. 3C, left heat map), especially the mitochondrial fission process. The observed up-regulation of *MID49*, *MID51*,

Table 1
Summary of miRNAs involved in the RLR pathway and mitochondrial dynamics

miRNA	miRNA expression (fold per control)		Luciferase activity, IFN- β (fold % per control)	Mitochondrial morphology
	Poly(I:C) stimulation	SeV infection		
hsa-miR-1250	229	2.5	16.1	Normal tubular
hsa-miR-143	138	14.7	40.8	Normal tubular
hsa-miR-302b-3p	4.3	2.9	3.5	Strong fragmentation
hsa-miR-338-5p	3.1	5.0	36.7	Normal tubular
hsa-miR-372	4.3	2.4	6.5	Strong fragmentation
hsa-miR-410	70.1	110	186	Normal tubular
hsa-miR-485-3p	287	212	45.6	Normal tubular
hsa-miR-520f-3p	17.3	5.4	7.8	Partial fragmentation
hsa-miR-922	16.3	13.0	71.5	Normal tubular

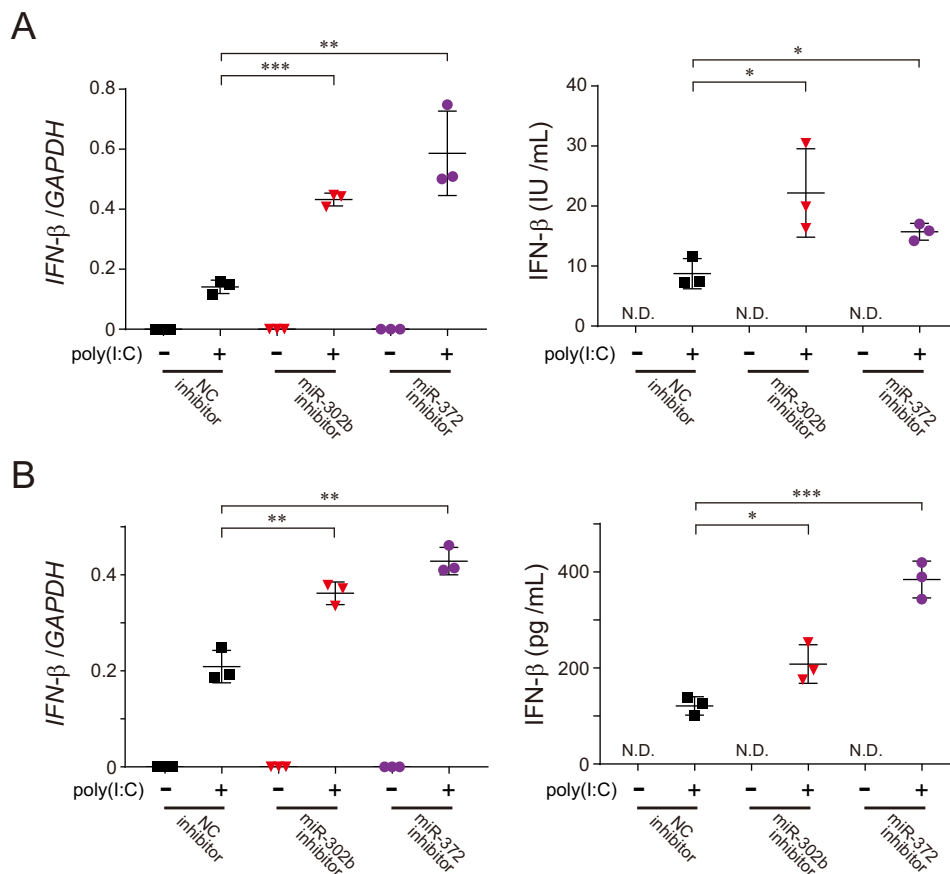


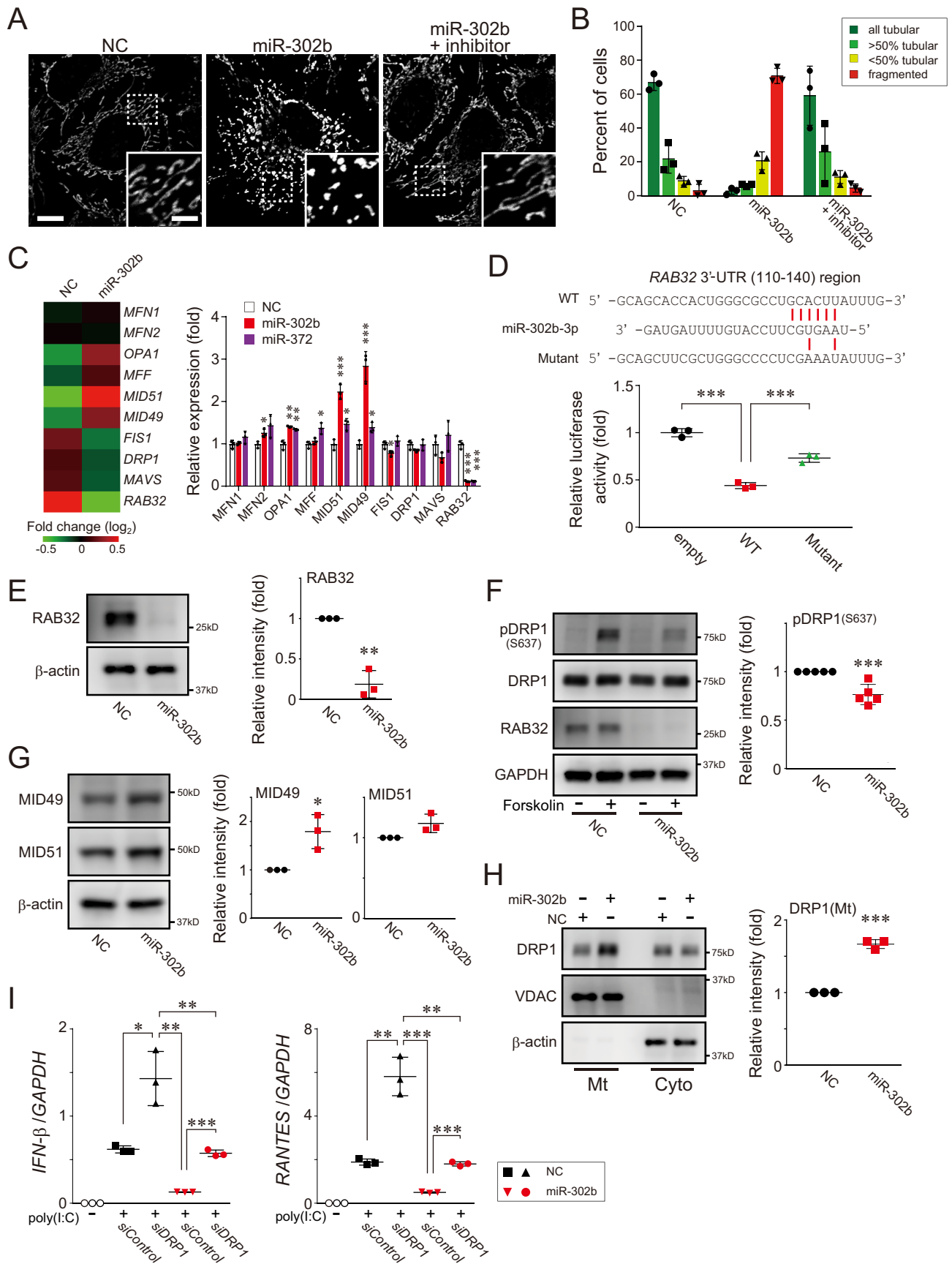
Figure 2. Both endogenous miR-302b and miR-372 regulate RLR-mediated signal transduction. A and B, HEK293 (A) or HAP-1 (B) cells were transfected with either the negative control (NC) or indicated miRNA inhibitors, and 48 h later, the cells were re-transfected with 2 μ g of poly(I:C) for 24 h, and the total RNAs from the cells were analyzed by qPCR for the expression of IFN- β (left), or the culture supernatants from the cells were analyzed by ELISA to measure IFN- β production (right). GAPDH was used as an internal control for the qPCR experiments. N.D., not detected. Data shown represent mean values \pm S.D. ($n = 3$). *, $p < 0.05$; **, $p < 0.01$; and ***, $p < 0.001$.

and MFF, adaptors for dynamin-related protein 1 (DRP1) (20), and significant down-regulation of Ras-related protein 32 (RAB32), all of which participate in mitochondrial fission (21–23), were further confirmed by gene expression analysis with qPCR in the miR-302b-transfected cells (Fig. 3C, right graph).

Indeed, the search for target genes against miR-302b using the program TargetScan revealed that RAB32 had a putative binding sequence in the 3'-UTR of the mRNA. To confirm the predicted results experimentally, we constructed a reporter plasmid in which the 3'-UTR region of RAB32(110–140) was cloned into a Renilla luciferase reporter gene. The results of the

reporter assay confirmed that the luciferase activity in HEK293 cells transfected with the miR-302b mimic was greatly attenuated when the WT RAB32 plasmid was co-transfected, whereas co-transfection with its mismatch-induced mutant plasmid had no effect (Fig. 3D and Fig. S2C). Consistent with these results, delivery of the miR-302b mimic into the cells significantly affected the abundance of endogenous RAB32 at both the mRNA (Fig. S2, D and E) and protein (Fig. 3E) levels. In addition, we observed that eliminating RAB32 through the action of miR-302b suppressed the phosphorylation of DRP1 at Ser⁶³⁷ (Fig. 3F), a hallmark of DRP1 activation (24), as seen in HEK293 cells treated with siRNA against RAB32 (Fig. S2F).

MicroRNAs regulate mitochondrial-mediated antiviral response



In contrast, HEK293 cells transfected with the miR-302b mimic also exhibited increased expression of the DRP1 adaptors MID49 and MID51, as confirmed by the increase in the amounts of their proteins in the cells (Fig. 3G). DRP1 recruitment in the mitochondrial fraction was sufficiently increased in an miR-302b-dependent manner (Fig. 3H), further indicating that our morphologic phenotype resulted in mitochondrial fragmentation (25). Together, these results highlighted the mechanism by which miR-302b is involved in mitochondrial fission via the DRP1-dependent pathway.

miR-302b also targets a mitochondrial transporter, SLC25A12, which modulates MAVS-mediated signaling

The presence of excess fragmented mitochondria ultimately leads to cellular signaling dysfunction, including the mitochondrial-mediated antiviral response (14). Therefore, we next evaluated whether arresting DRP1 activity in cells treated with an miR-302b mimic (Fig. S2G) would affect RLR-mediated signal transduction. As reported previously (14), depleting endogenous DRP1 in HEK293 cells through its specific siRNA enhanced the induction of both IFN-β and RANTES in response to poly(I-C) stimulation relative to that in control siRNA-transfected cells (Fig. 3I). However, the loss of DRP1 in cells treated with the miR-302b mimic also showed potential induction of immune responses compared with controls, but the recovery was only partial in the cells transfected with a negative control mimic (Fig. 3I, NC/siDRP1 versus miR-302b/siDRP1). These findings suggest that some other factors besides mitochondrial morphology are involved in the RLR pathway, leading us to explore the direct involvement in signal transduction.

Thorough analysis of our microarray data revealed that SLC25A12, a member of the solute carrier family, was intensively down-regulated in miR-302b-transfected HEK293 cells (Fig. 4A). As expected, SLC25A12 possessed a miR-302b-binding sequence in its 3'-UTR (Fig. 4B and Fig. S3A), whose low abundance of protein was experimentally confirmed in cells transfected with the miRNA mimic (Fig. 4C). Strikingly, the antiviral immune responses detected on the basis of the

expression of IFN-β and RANTES in HEK293 cells stimulated by poly(I-C) were significantly decreased in an SLC25A12-depleted condition (Fig. 4D). Knockdown of endogenous SLC25A12 in the cells similarly reduced IFN-β reporter activation in response to the overexpression of either RIG-I¹⁻²⁵⁰ or MAVS constructs (Fig. S3B). We also verified the antiviral immune function of SLC25A12 using SLC25A12-deficient HAP-1 cells (Fig. 4E). Because SLC25A12, an aspartate-glutamate transporter localized in the mitochondrial inner membrane (MIM) (26), is required for regulating antiviral signaling through MAVS, it is likely that SLC25A12 acts downstream of MAVS in the pathway.

SLC25A12 associates with MAVS in mitochondria

While exploring the mechanisms of action of SLC25A12, we found that the transporter co-immunoprecipitated with endogenous MAVS in HEK293 cells under physiologic conditions (Fig. 5A). We therefore performed a structure-function analysis to fill the topologic gap between SLC25A12 and MAVS. Using a co-immunoprecipitation approach, we mapped the region of SLC25A12 that interacts with MAVS via the C-terminal region (Fig. 5B) that faces the intermembrane space (IMS) with an unknown function (27). Consistent with the immunoprecipitation results, fluorescence microscopy confirmed the co-localization of both SLC25A12 and MAVS in HeLa cells (Fig. 5C). We explored additional molecules that might bridge SLC25A12 and MAVS at the IMS and found that prohibitins (PHB1 and PHB2), mitochondrial scaffolds localized in the MIM (28), associated with SLC25A12 (Fig. 5, A and D). We assume that SLC25A12, as a part of the PHB interactome (28), interacts with MAVS in mitochondria.

Interestingly, decreasing SLC25A12 in cells affected the structural features of the MAVS activation accompanied by RLR-mediated signal transduction, i.e. homotypic oligomerization (29, 30) at the MOM (Fig. 5, E and F), which further highlights the importance of the transporter in the activation of the signaling pathway. In addition, SLC25A12-specific siRNA had no effect on IFN-β reporter activation in

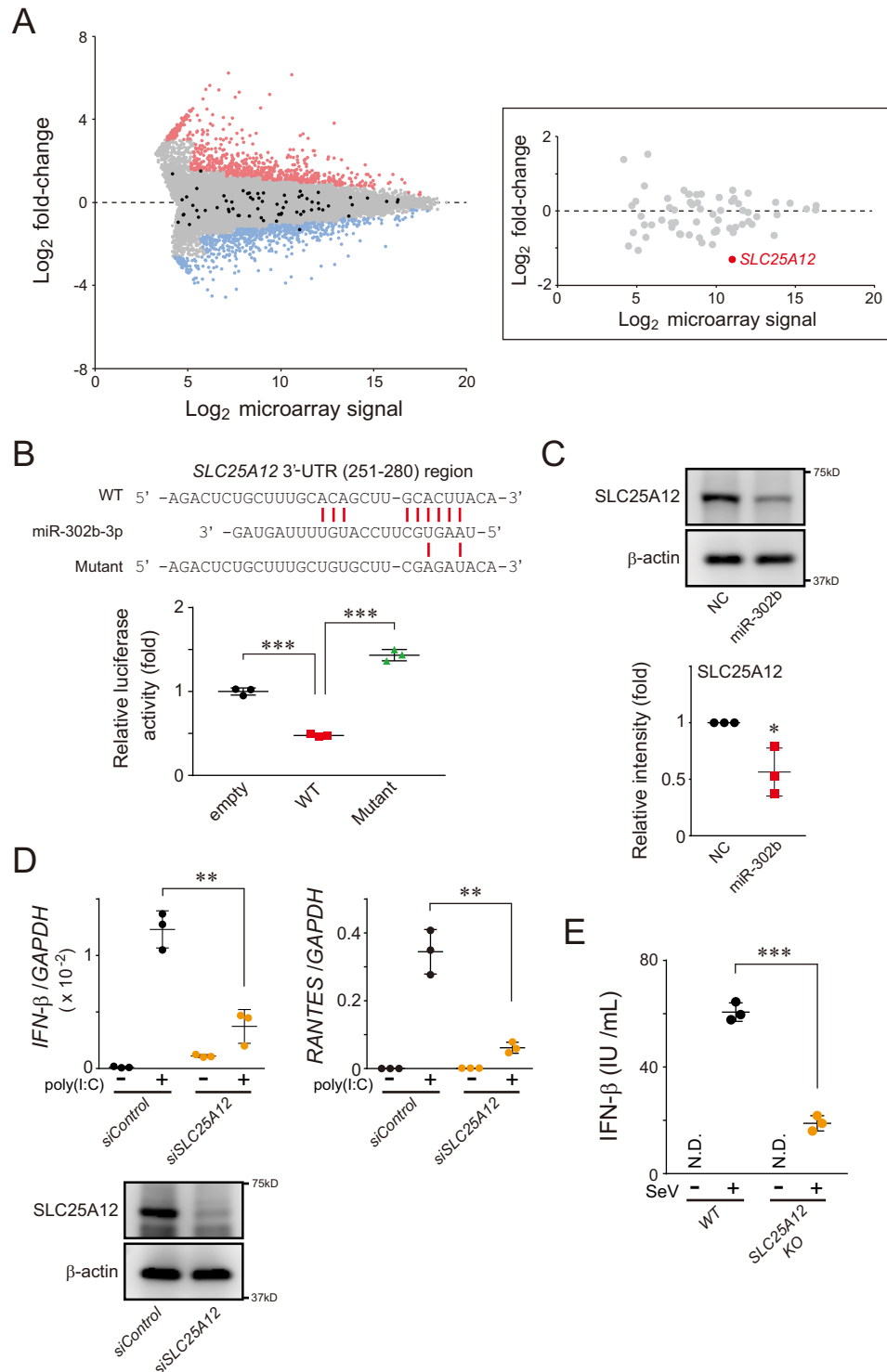
Figure 3. miR-302b promotes mitochondrial fission through a DRP1-dependent pathway. A, HeLa cells were transfected with either negative control (NC) or miR-302b mimics, and the mitochondrial morphology of the transfected cells was monitored 72 h later by immunofluorescence microscopy. Mitochondria in the cells were stained with an antibody against mtHSP70. The presence of an miR-302b-specific inhibitor rescued its defects in mitochondrial tubular networks (right, miR-302b + inhibitor). Each inset depicts a magnified image of the dashed-boxed area. Scale bar, 10 μm (inset, 5 μm). B, quantification of mitochondrial morphology in A. Cells were scored as one of four morphologic categories as depicted in the inset, and at least 200 cells were scored. Data shown represent mean values ± S.D. (n = 3). C, total RNAs were isolated from HEK293 cells post-transfection with either negative control (NC) or miR-302b mimics for 72 h, and microarray analysis was performed (n = 1). The heat map (left) compared the expression profile of mitochondrial dynamics-related genes and was generated by MeV software (45). The color indicates the distance from the median of each row. The right graph shows the gene expression profiles of the cells transfected either with miR-302b or miR-372 mimics for 72 h and analyzed by qPCR. NC, negative control mimic. The qPCR data shown represent mean values ± S.D. (n = 3). *, p < 0.05; **, p < 0.01; and ***, p < 0.001. D, HEK293 cells were transfected with either plasmid, psiCHECK-2 (empty), or psiCHECK-2 that cloned a 3'-UTR region of RAB32(110–140), together with an miR-302b mimic. The transfected cells were analyzed 24 h later for reporter gene-dependent luciferase activity. Top, predicted base-pairing between miR-302b-3p and the RAB32 target, and the positions of paired sites are indicated by the red bars. Data shown represent mean values ± S.D. (n = 3). ***, p < 0.001. E, HEK293 cells were transfected with the negative control or miRNA mimics, and the whole-cell lysates were analyzed by Western blotting with an antibody against RAB32 (left). The band intensity of RAB32 was measured with QuantiStudio and normalized to the intensity of β-actin (right) (data shown represent mean values ± S.D. (n = 3)). **, p < 0.01. F, HeLa cells were transfected with the negative control or miRNA mimics and 72 h after transfection, DRP1 phosphorylation (Ser⁶³⁷) levels of forskolin-stimulated cells were analyzed by Western blotting (left). The band intensity of pDRP1 (S637) was measured and normalized to the intensity of GAPDH (right) (data shown represent mean values ± S.D. (n = 5)). ***, p < 0.001. G, similar to E, except that the expression levels of MID49 and MID51 were analyzed by Western blotting. Data shown represent mean values ± S.D. (n = 3). *, p < 0.05. H, similar to E, except that the endogenous DRP1 localization in cytosolic (Cyto) and mitochondrial (Mt) fractions isolated from the cells was analyzed by Western blotting. Data shown represent mean values ± S.D. (n = 3). ***, p < 0.001. I, HEK293 cells were transfected with either the negative control or miRNA mimics, together with the DRP1 siRNA (versus siControl) for 48 h. The transfected cells were then stimulated with poly(I-C) delivery into cells, and the expression of IFN-β, RANTES, and GAPDH (internal control) was measured by qPCR post poly(I-C) transfection (2 μg). Data shown represent mean values ± S.D. (n = 3). *, p < 0.05; **, p < 0.01; and ***, p < 0.001.

MicroRNAs regulate mitochondrial-mediated antiviral response

response to the overexpression of TANK-binding kinase 1 (TBK-1) (Fig. S3B), a kinase that targets IRF-3, despite the fact that the effector acts downstream of MAVS (9). On the basis of these findings, we propose a model in which SLC25A12 inhibits the RLR pathway downstream of MAVS (and/or at the same level) and upstream of the kinase TBK-1.

miR-302b regulates mitochondrial metabolism via SLC25A12, which controls antiviral responses

The results described above prompted us to investigate the functional role of SLC25A12 in the regulation of the antiviral response. Because SLC25A12 is a member of the malate-aspartate NADH shuttle (31, 32), we assessed its ability to transfer reducing equivalents. Treatment with the miR-302b mimic



significantly decreased the level of NADH in HEK293 cells without changing NAD, resulting in an ~50% greater NAD/NADH ratio (Fig. 6A), which indicated impaired mitochondrial metabolism. Metabolome analysis of the miRNA-transfected cells further revealed that the amounts of aspartate, malate, and pyruvate were similarly decreased in cells treated with the miR-302b mimic, while the amount of lactate was increased (Fig. 6B). Consistent with our observations, a decrease in the oxygen consumption rate (OCR) indicated that the miR-302b-targeted mitochondria in the cells became less active (Fig. 6C and Fig. S4A), and the cellular metabolism shifted to glycolytic conditions (Fig. 6D).

We confirmed that the observed regulation of mitochondrial-related metabolites was mainly due to the function of SLC25A12 on the basis of diminishing SLC25A12 in cells with a lower OCR (Fig. 6E and Fig. S4B). To explore whether these metabolic changes in the mitochondria correlated with RLR pathway activation, we performed a signaling assay. As expected, the immunodeficiency observed in the *siSLC25A12*-treated HEK293 cells was significantly recovered by adding aspartate to the media (Fig. 6F), similar to the OCR patterns in *SLC25A12*-deficient cells (Fig. S4C). In addition to the substantial contribution of SLC25A12 to mitochondrial metabolism, we identified that miR-302b targets mitochondrial pyruvate carrier 1 (MPC1) (Fig. S4, D and E) (33, 34), and changes in the amount of its protein partially affect mitochondrial respiration (Fig. S4B). Taken together, these findings indicate that the absence of mitochondrial metabolites leads to defective mitochondrial-mediated antiviral signaling.

Discussion

MicroRNAs are known to be involved in various cellular functions, and several miRNAs are triggered by an immune response to induce IFNs (35, 36). Here, we report that two miRNAs, miR-302b and miR-372, potentially attenuate virus-triggered induction of IFN- β and pro-inflammatory cytokines by manipulating mitochondrial functions, such as mitochondrial dynamics and metabolism.

Although much attention has been focused on the identification and characterization of signaling molecules that activate and/or inactivate mitochondrial-mediated antiviral innate immunity, our study explored the mechanistic basis of how these molecules are regulated at the mRNA level and the involvement of the translated products in the signaling event. On the basis of our findings, we propose that miR-302b and

miR-372 regulate mitochondrial-mediated antiviral responses by controlling the expression of mitochondrial proteins (such as SLC25A12) to prevent excessive progression of the antiviral response (Fig. 6G). In addition to revealing the mechanistic action of these miRNAs, the findings of this study may pave the way for understanding an unexpected role of these miRNAs as a therapeutic target for attenuating excess inflammation, such as a cytokine storm because of their high potency for down-regulating pro-inflammatory cytokines.

Finally, a previous study revealed that miR-302a, a member of the miR302 family encoded in the human miR302–367 cluster (37), suppresses influenza A virus, an RNA virus of the Orthomyxoviridae family, stimulates interferon regulatory factor-5 (IRF-5) expression, and inhibits the production of IFNs and inflammatory cytokines (38). The seed sequences of miR-302b and miR-372 are homologous to that of miR-302a, indicating that both miR-302b and miR-372 would likely act as negative regulators of IRF-5 to prevent the induction of a cytokine storm, as in the case of miR-302a. Therefore, miR-302b and miR-372 may function as potential regulators of the influenza A virus-induced cytokine storm and provide a candidate target for the treatment of influenza A virus infection.

Experimental procedures

Reagents

Poly(I-C) was purchased from InvivoGen (San Diego, CA), and enzyme-linked immunosorbent assay (ELISA) kits for human IFN- β were supplied by Kamakura Techno-Science Inc. (Kanagawa, Japan) and R&D Systems (Minneapolis, MN). All other reagents were biochemical research grade.

Cell lines and viruses

HEK293, HeLa, A549, and MRC-5 cells were maintained in Dulbecco's modified Eagle's medium (Gibco BRL) supplemented with 1% L-glutamine, penicillin (100 units/ml)-streptomycin (100 μ g/ml), and 10% fetal bovine serum at 5% CO₂ and 37 °C. The human *SLC25A12* knockout HAP-1 cell line edited by the CRISPR/Cas system was obtained from Horizon Discovery (Cambridge, UK) and maintained in Iscove's modified Dulbecco's medium (Gibco BRL) supplemented with 1% GlutaMAX, penicillin (100 units/ml)-streptomycin (100 μ g/ml), and 10% fetal bovine serum at 5% CO₂ and 37 °C. Sendai virus Cantell strain was purchased from the American Type Culture Collection (Manassas, VA).

Figure 4. miR-302b modulates SLC25A12 expression, which is involved in attenuating the mitochondrial-mediated antiviral response. A, representative MA plot of the microarray data. The x axis represents the log₂ transform of the microarray signals, and the y axis represents the log₂ transform of the fold-change of each gene in HEK293 cells transfected between negative control and miR-302b mimics (*n* = 1). Expression changes greater or less than 2-fold are considered as hits and are indicated as red and blue dots, respectively. Genes annotated as known SLC25 family members are indicated in black, and the inset on the right shows the highlight of only the SLC25 family position in which the SLC25A12 is indicated in red. B, HEK293 cells were transfected with either psiCHECK-2 (empty) or psiCHECK-2 that contained a 3'-UTR region of SLC25A12(251–280), together with miR-302b mimic. Transfected cells were analyzed 24 h later for reporter gene-dependent luciferase activities. Top, predicted base-pairing between miR-302b-3p and the target gene, and the positions of paired sites are indicated by the red bars. Data shown represent mean values \pm S.D. (*n* = 3), ***, *p* < 0.001. C, HEK293 cells were transfected with the negative control (NC) or miR-302b mimics, and whole-cell lysates were analyzed 72 h later by Western blotting with an antibody against SLC25A12 (top). Band intensity was measured with ImageQuant TL and normalized to the intensity of β -actin (bottom) (data shown represent mean values \pm S.D. (*n* = 3)). *, *p* < 0.05. D, siRNA-treated HEK293 cells (*siSLC25A12*) were transfected with 2 μ g of poly(I-C) for 24 h, and the total RNA from the cells was analyzed by qPCR for the expression of IFN- β , RANTES, and GAPDH (internal control). Data shown represent mean values \pm S.D. (*n* = 3). **, *p* < 0.01. The efficiency of SLC25A12 knockdown was confirmed by Western blot analysis with an antibody against SLC25A12 (bottom). E, SLC25A12 knockout and its parental (WT) HAP-1 cell lines were infected with SeV (4 HAU/ml) for 24 h, and IFN- β production was measured by ELISA. N.D., not detected. Data shown represent mean values \pm S.D. (*n* = 3). ***, *p* < 0.001.

MicroRNAs regulate mitochondrial-mediated antiviral response

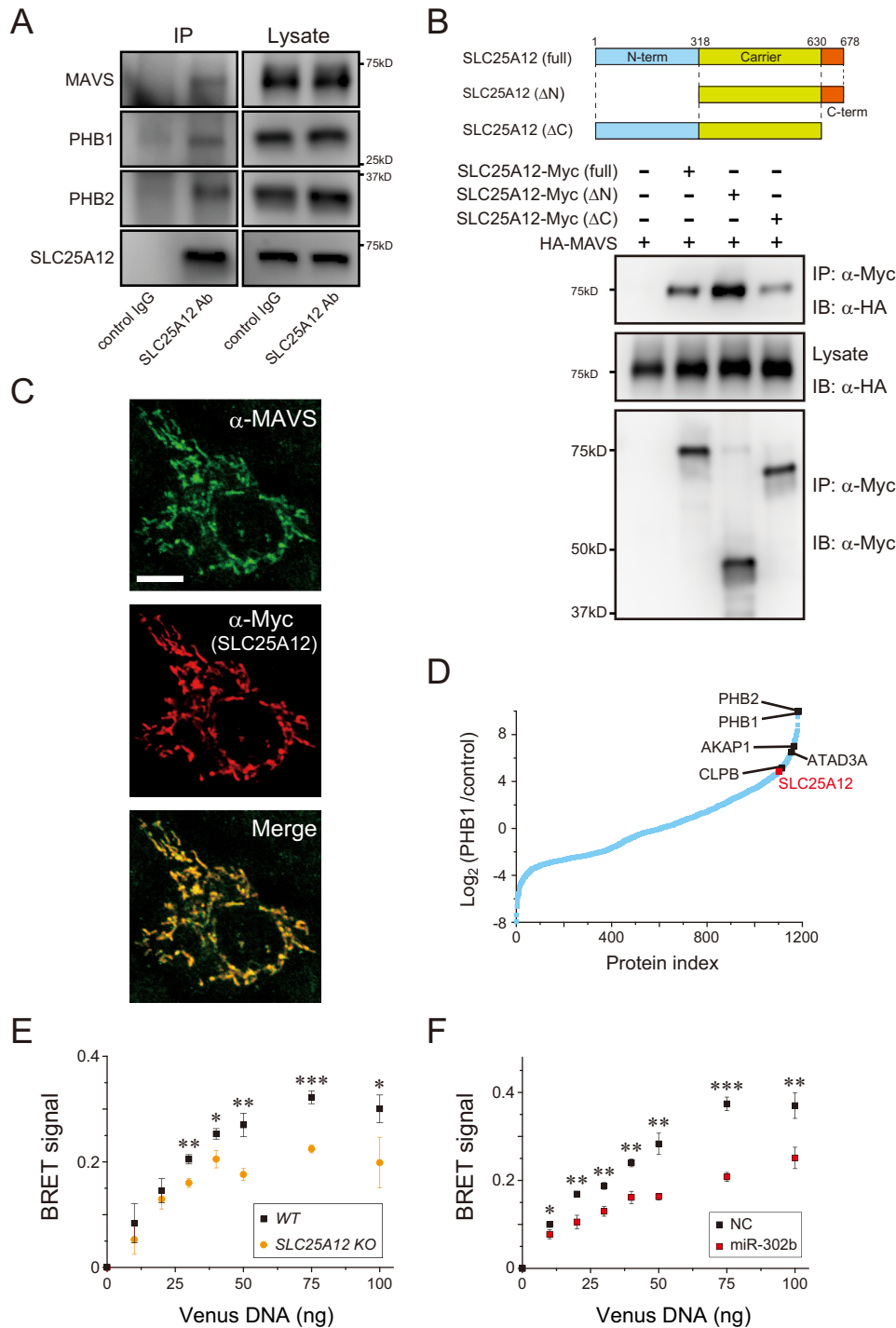
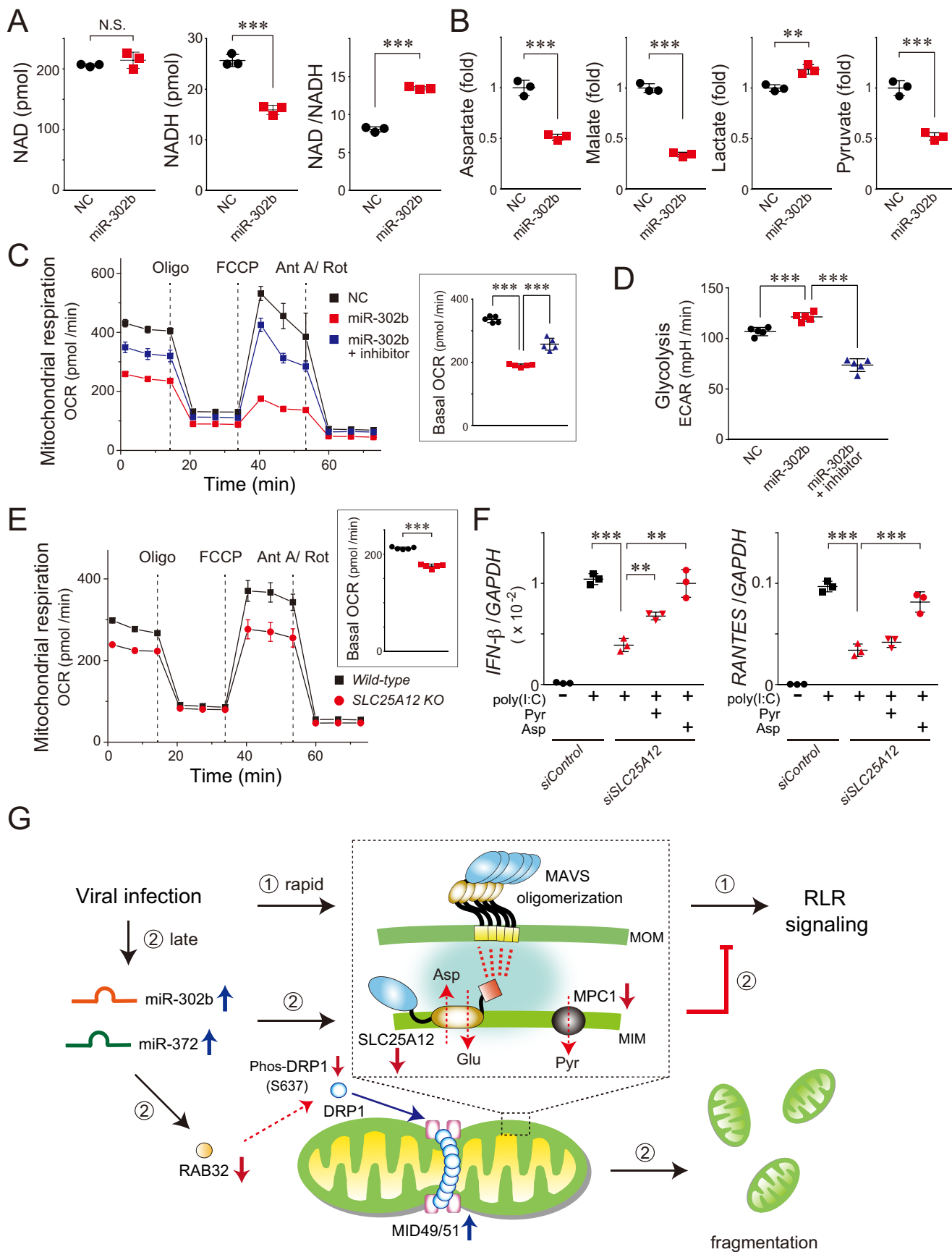


Figure 5. SLC25A12 associates with the mitochondrial antiviral signaling protein MAVS. A, interaction of endogenous SLC25A12 with MAVS and PHB complexes. Lysates of HEK293 cells (*right*) were subjected to immunoprecipitation (*IP*, *left*) with anti-SLC25A12 antibody or control IgG followed by analysis of Western blottings with antibodies against MAVS, PHB1, and PHB2. B, HEK293 cells were co-transfected with the indicated combinations of plasmids encoding HA-tagged MAVS and Myc-tagged SLC25A12 variants (*top*). Western blottings of samples immunoprecipitated (*IP*) with an anti-Myc or post-nuclear cell lysates (*Lysate*) were analyzed by immunoblotting (*IB*) with either the anti-HA or the anti-Myc antibodies. C, immunofluorescence microscopy of HeLa cells transfected with a plasmid encoding Myc-tagged SLC25A12. Cells were visualized with endogenous MAVS (Alexa Fluor 488, *green*) and SLC25A12 (Cy3, *red*). Scale bar, 10 μ m. D, interaction between PHB1 and SLC25A12. A total of 1183 proteins re-analyzed using our previous PHB1 interactors (28) were plotted according to the abundance ratios (\log_2) of PHB1/control against individual proteins (*Protein index*) sorted by their ratios in ascending order. Interactions, such as those of PHB1 and CLPB, were confirmed as a positive control. E, SLC25A12 knockout (*orange*) or WT (*black*) HAP-1 cells were each co-transfected with 10 ng of NLuc-MAVS expression plasmid with increasing amounts (0–100 ng) of Venus-tagged MAVS plasmid and analyzed 24 h later using a BRET saturation assay (30). Data shown represent mean values \pm S.D. ($n = 3$). *, $p < 0.05$; **, $p < 0.01$, and ***, $p < 0.001$. F, similar to E, except that the miRNA mimic-treated HEK293 cells were used. Data shown represent mean values \pm S.D. ($n = 3$). *, $p < 0.05$; **, $p < 0.01$, and ***, $p < 0.001$.



MicroRNAs regulate mitochondrial-mediated antiviral response

Antibodies

Anti-SLC25A12 (ab200201, 1:4000), anti-IRF3 (pSer³⁸⁶; ab76493, 1:2000), anti-REA/PHB2 (ab181838, 1:5000) rabbit mAbs, anti-MAVS (ab31334, 1:1000) rabbit polyclonal antibody (pAb), and anti-c-Myc (9E10, 1:1000) mouse mAb were purchased from Abcam (Cambridge, MA). Anti- β -actin (sc-47778, 1:1000) mouse mAb was purchased from Santa Cruz Biotechnology (Dallas, TX). Anti-MID49 (16413-1-AP, 1:1000) and anti-MID51 (20164-1-AP, 1:1000) rabbit pAbs were purchased from Proteintech (Rosemont, IL). Anti-RAB32 (SAB4200086, 1:1000) rabbit pAb and anti-hemagglutinin (HA; HA-7, 1:2000) mAb were purchased from Sigma. Anti-DRP1 (D6C7, 1:1000), anti-DRP1 (pSer⁶³⁷; D3A4, 1:1000), anti-MPC1 (D2L9I, 1:1000), anti-GAPDH (14C10 biotinylated, 1:1000), anti-VDAC (D73D12, 1:1000) rabbit mAbs, and anti-PHB1 (catalog no. 2426, 1:1000) rabbit pAb were supplied from Cell Signaling Technology (Danvers, MA). Anti-mitochondrial heat-shock protein 70 (mtHSP70; JG1, 1:1000) mouse mAb, anti-MAVS (PA5-17256, 1:100) rabbit pAb, and the Alexa Fluor 568 (catalog no. A11031, 1:400)-conjugated goat anti-mouse IgG pAb were purchased from Thermo Fisher Scientific (Waltham, MA). A list of all Abs used in this study is provided in the Key Resources Table S1.

Plasmids

The plasmids encoding human MAVS variants and hRIG-I¹⁻²⁵⁰ were described previously (30, 39). To construct reporter plasmids for the SLC25A12, Rab32, and MPC1 target sequence in 3'-UTR, synthetic oligonucleotides encoding 3'-UTR residues containing a 5' XhoI restriction site, and their antisense oligonucleotides containing a 3' NotI site were cloned into a psiCHECK-2 plasmid (Promega, Madison, WI). The oligonucleotides used for inserts were as follows: sense, 5'-tcgagagactctgctttgcacagcttgcaactacagc-3', and antisense, 5'-ggccgctgt-aagtcaagctgtgcaagcagagcttc-3' (SLC25A12 3'-UTR); sense, 5'-tcgaggcagcaccactggcgctgcaactatttggc-3', and antisense, 5'-ggccgcaataagtgcaggcgccagtggtgctgcc-3' (RAB32 3'-UTR); and sense, 5'-tcgaggaacaaaattgtaacactagcacttaaggc-3', and antisense, 5'-ggccgcttaagtgtactgtgttacaattttgtcc-3' (MPC1 3'-UTR).

RNAi and miRNA mimic/inhibitor introduction

For RNAi and miRNA mimic/inhibitor introduction experiments, siRNAs and miRNA mimics/inhibitors were purchased

from Qiagen (GeneSolution siRNA) and Ambion (mirVana miRNA mimics and inhibitors), respectively. For siRNAs, we used *SLC25A12* (SI00054929), *RAB32* (SI00092246), *MPC1* (SI04153415), and 5'-AUUUACCCCAUUCUUCUGCTT-3' sequence against DRP1. AllStars Negative Control siRNA was used for the negative controls. For miRNA mimics and their inhibitors, miR-302b mimic (MC10081), miR-302b inhibitor (MH10081), miR-372 mimic (MC10165), and miR-372 inhibitor (MH10165) were used in the study. mirVana miRNA mimic (negative control no. 1) and mirVana miRNA Inhibitor (negative control no. 1) were used for each negative control, respectively. In the experiments, HEK293 cells were transfected with either 10 nM siRNA or miRNA (final concentration) using Lipofectamine RNAiMAX (Thermo Fisher Scientific) following the manufacturer's protocols. At 48 h after treatment, the cells were used for each functional assay.

Reverse transcription qPCR

Total RNA was isolated from cells with an miRNeasy mini kit (Qiagen, Hilden, Germany) or a Maxwell 16 LEV simplyRNA cell kit (Promega) according to the manufacturer's protocol, and 500 ng of total RNA was reverse-transcribed with a QuantiTect reverse transcription kit (Qiagen) or TaqMan MicroRNA reverse transcription kit (Thermo Fisher Scientific) to generate cDNAs. Real-time PCR assays were performed with a TaqMan Gene Expression assay using the indicated probes.

ELISA

Production of IFN- β was measured with species-specific ELISA reagents for human IFN- β from Kamakura Techno-Science Inc. and R&D Systems.

Confocal microscopy

Cells were plated on coverslips in 12-well plates (5×10^4 cells/well). The following day, the cells were fixed with 4% paraformaldehyde for 15 min, permeabilized with 0.2% Triton X-100 in 1 \times PBS (pH 7.2), and blocked with 5% fetal bovine serum. Mitochondria were visualized by using either mitochondrial-targeted red fluorescent protein (12) (mito-RFP; Fig. 1C) or staining with anti-mtHSP70 (Fig. 3A and Fig. S2, A and G) or MAVS (Fig. 5C) pAbs followed by Alexa Fluor 568-conjugated polyclonal and Alexa Fluor 488-conjugated polyclonal secondary Abs, respectively. Cells were imaged with a C2+ confocal microscope (Nikon Instruments Inc.).

Figure 6. miR-302b targets SLC25A12 to disrupt mitochondrial metabolism linked to the antiviral responses. A, NAD and NADH levels (pmol/10⁶ cells) in HEK293 cells transfected with miR-302b mimic were analyzed 72 h later by LC-MS/MS. The right graph shows the NAD/NADH ratio. *N.S.*, not significant. Data shown represent mean values \pm S.D. ($n = 3$). ***, $p < 0.001$. B, mitochondria-related metabolites in the miR-302b mimic-transfected HEK293 cells analyzed 72 h later by GC/MS. The aspartate, malate, and pyruvate levels were each significantly decreased, whereas the lactate level was increased. Data shown represent mean values \pm S.D. ($n = 3$). **, $p < 0.01$ and ***, $p < 0.001$. C, OCR of HEK293 cells transfected with the miR-302b mimic (\pm inhibitor) measured using a Seahorse XFe96 Analyzer. *Inset*: basal OCR of each transfected cell. The injection order of oligomycin (*Oligo*), FCCP, and antimycin A/rotenone (*Ant A/Rot*) is indicated. Data shown represent mean values \pm S.D. ($n = 5$). ***, $p < 0.001$. D, extracellular acidification rate of HEK293 cells transfected with the miR-302b mimic (\pm inhibitor) was measured using the Seahorse XFe96 Analyzer. Data shown represent mean values \pm S.D. ($n = 5$). ***, $p < 0.001$. E, similar to C, except that the representative respiration of the *SLC25A12* knockout and its WT HAP-1 cells was measured. Data shown represent mean values \pm S.D. ($n = 5$). ***, $p < 0.001$. F, siRNA-treated HEK293 cells (*siSLC25A12*) were transfected with 2 μ g of poly(I-C) for 24 h, and the total RNA from the cells was analyzed by qPCR for the expression of *IFN- β* , *RANTES*, and *GAPDH* (internal control). At the time of the poly(I-C) transfection, either pyruvate (*Pyr*, 2.5 mM) or aspartate (*Asp*, 10 mM) was added to the medium of the *siSLC25A12*-treated cells. Data shown represent mean values \pm S.D. ($n = 3$). **, $p < 0.01$ and ***, $p < 0.001$. G, model of miRNAs that control RLR-mediated antiviral signaling. Cellular innate immune responses to RNA virus infection result in the rapid activation of signaling molecules, including MAVS oligomerization (*inset*) and the formation of signalosomes on the MOM, ultimately facilitating the RLR-signaling pathway (Ⓢ). In this process, we assume that SLC25A12, as a part of the PHB interactome (*inset*, highlighted with blue background) (28), interacts with MAVS in mitochondria that have a critical role in MAVS oligomerization. At longer times post-infection (\sim 24 h), miR-302b (and also miR-372) is up-regulated in the cells, which promotes mitochondrial fission through the DRP1-dependent pathway and also impairs mitochondrial metabolism (Ⓣ). We propose that the miRNAs undergo sequential negative regulations following viral infection, a process that is critical for terminating excess RLR signaling.

Luciferase reporter assay

HEK293 cells were plated in 96-well plates (3×10^4 cells/well). On the same day, the cells were co-transfected with 40 ng of luciferase reporter plasmid (p125luc or pELAM), 4 ng of *Renilla* luciferase internal control vector phRL-TK (Promega), and each of the indicated expression plasmids or poly(I-C) (500 ng) using Lipofectamine 2000 reagent (Invitrogen) following the manufacturer's protocols. The cells were harvested 24 h after transfection and analyzed using a Dual-Glo Luciferase Assay System (Promega). Relative luciferase activity was calculated by normalizing luciferase activity by the *Renilla* luciferase activity expressed in internal control plasmids and dividing by the normalized value of the control in which only an empty vector (pcDNA3.1) was transfected. Each experiment replicated at least three independent reproducible results. The p125luc and pELAM reporter plasmids were provided by T. Taniguchi (University of Tokyo, Japan) and T. Seya (Hokkaido University, Japan), respectively.

BRET assay

BRET experiments were performed as described previously (30) with minor modifications. HEK293 cells were transfected with miRNA mimics. At 48 h after the treatment, the miRNA mimic-transfected cells were plated in a 96-well microplate and transfected with 5 ng of Nanoluc-tagged MAVS plasmid and increasing amounts of Venus-tagged MAVS constructs using Lipofectamine 2000 at the same time. Twenty hours after transfection, 0.1 μ l of Nanoluc substrate was added to each well, followed by 1 min of gentle mixing, and luminescence was measured simultaneously for the donor ($\lambda_{em} = 460$ nm; short wavelength) and acceptor ($\lambda_{em} = 515$ nm; long wavelength).

Immunoprecipitation

Co-immunoprecipitation experiments were performed as described previously (39) with minor modifications. HEK293 cells at 80% confluence were transiently transfected with the appropriate plasmids (1.25 μ g each) in a six-well plate using the FuGENE HD transfection reagent (Promega). The following day, the cells were lysed with 1 ml of radioimmunoprecipitation assay (RIPA) buffer with a protease inhibitor mixture, and the clarified supernatants were incubated overnight at 4 °C with anti-c-Myc-agarose beads (Sigma). After four washes with 1 \times PBS (pH 7.2), the immunoprecipitates were resolved by 10% SDS-PAGE and analyzed by Western blotting with a mAb against HA followed by a horseradish peroxidase-conjugated antibody against mouse IgG (Cell Signaling Technology). To immunoprecipitate endogenous MAVS, PHB1, or PHB2, HEK293 cells in a 10-cm dish were washed once with 1 \times PBS (pH 7.2), lysed with 2 ml of RIPA buffer containing protease inhibitor mixture, and the clarified supernatants were incubated with 10 μ g of anti-SLC25A12 rabbit mAb followed by incubation overnight at 4 °C with 25 μ l of protein A-Sepharose beads. The beads were washed four times with 1 \times PBS (pH 7.2), and the immunoprecipitates were resolved by 10% SDS-PAGE and immunoblotted with each Ab.

Mitochondrial fractionation

The cells were harvested and washed once with cold 1 \times PBS (pH 7.2) and resuspended in 700 μ l of homogenization buffer (20 mM HEPES (pH 7.4), 70 mM sucrose, and 220 mM mannitol) by 30 strokes in a Dounce homogenizer. The homogenate was centrifuged at $800 \times g$ for 10 min, and the resulting supernatant was further centrifuged at $10,000 \times g$ for 10 min at 4 °C to precipitate the crude mitochondrial fraction. The resultant supernatant was centrifuged at $20,000 \times g$ for 30 min to obtain the cytosol fraction. The crude mitochondrial fraction was resuspended in homogenization buffer and applied to a discontinuous Percoll gradient comprising 80, 52, and 26% (w/v) Percoll diluted in homogenization buffer. Centrifugation was performed at $43,000 \times g$ for 45 min. The purified mitochondrial fraction was recovered from the interface between the 52 and 26% (w/v) Percoll.

Mitochondrial respiration and glycolysis analysis

Mitochondrial respiration and glycolysis analysis were performed using the Seahorse XFe96 Analyzer (Agilent Technologies, Santa Clara, CA). HEK293 cells were seeded on XFe96 spheroid microplates (6×10^4 cells/well) the day before the experiment and analyzed using the Seahorse XF Cell Mito Stress Test kit or the Seahorse XF Glycolysis Stress Test kit according to the manufacturer's protocols. Before measuring mitochondrial OCR, the culture medium was replaced with XF base medium supplemented with 1 mM pyruvate, 10 mM glucose, and 2 mM L-glutamine. First, the baseline values were measured three times, and the mitochondrial OCR in each state was then measured three times after adding the mitochondrial respiratory chain inhibitors to the cells. Oligomycin (2 μ M), FCCP (1.5 μ M), and rotenone/antimycin A (0.5 μ M) were used as mitochondrial respiratory chain inhibitors. The obtained data were analyzed using Wave 2.4.0 software (Agilent Technologies).

Microarray analysis

Total RNA was isolated from cells transfected with the negative control miRNA mimic or miR-302b mimic 72 h later using an miRNeasy mini kit (Qiagen) according to the manufacturer's protocol. RNA samples were quantified using an ND-1000 spectrophotometer (NanoDrop Technologies, Wilmington, DE), and the quality was confirmed with an Experion System (Bio-Rad). The cRNA was amplified, labeled (low-input Quick Amp labeling kit), and hybridized to the SurePrint G3 Human GE version 3 8×60 K microarray according to the manufacturer's instructions (Agilent Technologies). All hybridized microarray slides were scanned by an Agilent scanner (Agilent Technologies). Relative hybridization intensities and background hybridization values were calculated using Agilent Feature Extraction Software (version 9.5.1.1). Raw signal intensities and flags for each probe were calculated from the hybridization intensities (gProcessedSignal) and spot information (gIsSaturated, etc.) according to the procedures recommended by Agilent. The raw signal intensities of four samples were normalized by a quantile algorithm with the "preprocessCore" library package (40) of the Bioconductor software (41). To identify up-regulated or down-regulated genes, we cal-

MicroRNAs regulate mitochondrial-mediated antiviral response

culated the Z-scores (42) and ratios (nonlog scaled fold-change) from the normalized signal intensities of each probe to compare between control and experimental samples, and we established criteria for regulated genes: Z-score ≥ 2.0 and ratio ≥ 1.5 -fold for up-regulated genes, and Z-score ≤ -2.0 and ratio ≤ 0.66 for down-regulated genes, respectively. The GEO accession number for the microarray data reported in the paper is GSE129615.

Metabolite measurement for LC-MS and GC-MS

Metabolites were extracted from cultured cell pellets using water/methanol/chloroform (1:1:2), and the aqueous phase was preserved. For LC/MS experiments, the dried metabolites were dissolved in 50 μ l of LC/MS-grade water (Wako Pure Chemical Industries, Osaka, Japan) and then filtered with a 0.45- μ m Millex filter unit (Merck Millipore). For GC-MS experiments, derivatization of the samples was carried out in two steps using methoximation and *N*-methyl-*N*-trimethylsilyltrifluoroacetamide + 1% trimethylchlorosilane (Pierce) as described previously. Levels of NAD and NADH were determined by multiple reaction monitoring using an Agilent 6460 Triple Quad mass spectrometer coupled with an Agilent 1290 HPLC system. The MS settings and chromatographic conditions used were described previously (43). Tricarboxylic acid cycle intermediates were analyzed by selected ion monitoring using an Agilent 5977 MSD Single Quad mass spectrometer coupled with Agilent 7890 gas chromatograph as described previously (44). Metabolite amounts were calculated by the integrated sum of the area using Mass Hunter Quantitative software (Agilent Technologies).

Statistical analysis

An analysis of variance test (GraphPad Prism) was used for the statistical analyses. We considered different populations of cells to be biologic replicates; aliquoting or repeated measurements of a cell population was considered to represent technical replicates. We performed at least three independent reproducible results for most key experiments, although we did not perform explicit power calculations. Data are presented as the mean \pm S.D. Statistical significance was assessed by Student's *t* test. A *p* value of less than 0.05 was considered statistically significant.

Author contributions—K. Yasukawa and T. K. conceptualization; K. Yasukawa, K. Yaku, T. N., and T. K. data curation; K. Yasukawa, D. K., K. Yaku, T. N., and T. K. formal analysis; K. Yasukawa and T. K. validation; K. Yasukawa, D. K., and T. K. methodology; K. Yasukawa and T. K. writing-original draft; K. Yasukawa and T. K. project administration; D. K., K. Yaku, T. N., and T. K. investigation; T. K. resources; T. K. supervision; T. K. funding acquisition; T. K. visualization; T. K. writing-review and editing.

Acknowledgments—We are grateful to Koji Okamoto (Osaka University, Japan) for valuable comments on the study. We thank Hidetaka Kosako (Tokushima University, Japan) for helpful discussion on the PHB complexes. We appreciate Yuko Fuchigami (Kyushu University) for technical assistance with DNA cloning and sequencing.

References

1. Ambros, V. (2004) The functions of animal microRNAs. *Nature* **431**, 350–355 [CrossRef Medline](#)
2. Wienholds, E., and Plasterk, R. H. (2005) MicroRNA function in animal development. *FEBS Lett.* **579**, 5911–5922 [CrossRef Medline](#)
3. Mendell, J. T., and Olson, E. N. (2012) MicroRNAs in stress signaling and human disease. *Cell* **148**, 1172–1187 [CrossRef Medline](#)
4. Li, Y., and Shi, X. (2013) MicroRNAs in the regulation of TLR and RIG-I pathways. *Cell. Mol. Immunol.* **10**, 65–71 [CrossRef Medline](#)
5. Yarbrough, M. L., Zhang, K., Sakthivel, R., Forst, C. V., Posner, B. A., Barber, G. N., White, M. A., and Fontoura, B. M. (2014) Primate-specific miR-576-3p sets host defense signalling threshold. *Nat. Commun.* **5**, 4963 [CrossRef Medline](#)
6. Ingle, H., Kumar, S., Raut, A. A., Mishra, A., Kulkarni, D. D., Kameyama, T., Takaoka, A., Akira, S., and Kumar, H. (2015) The microRNA miR-485 targets host and influenza virus transcripts to regulate antiviral immunity and restrict viral replication. *Sci. Signal.* **8**, ra126 [CrossRef Medline](#)
7. Kawai, T., and Akira, S. (2006) Innate immune recognition of viral infection. *Nat. Immunol.* **7**, 131–137 [CrossRef Medline](#)
8. Meylan, E., and Tschopp, J. (2006) Toll-like receptors and RNA helicases: two parallel ways to trigger antiviral responses. *Mol. Cell* **22**, 561–569 [CrossRef Medline](#)
9. Seth, R. B., Sun, L., Ea, C. K., and Chen, Z. J. (2005) Identification and characterization of MAVS, a mitochondrial antiviral signalling protein that activates NF- κ B and IRF3. *Cell* **122**, 669–682 [CrossRef Medline](#)
10. Koshiba, T. (2013) Mitochondrial-mediated antiviral immunity. *Biochim. Biophys. Acta* **1833**, 225–232 [CrossRef Medline](#)
11. Koshiba, T., Yasukawa, K., Yanagi, Y., and Kawabata, S. (2011) Mitochondrial membrane potential is required for MAVS-mediated antiviral signaling. *Sci. Signal.* **4**, ra7 [CrossRef Medline](#)
12. Yoshizumi, T., Ichinohe, T., Sasaki, O., Otera, H., Kawabata, S., Mihara, K., and Koshiba, T. (2014) Influenza A virus protein PB1-F2 translocates into mitochondria via Tom40 channels and impairs innate immunity. *Nat. Commun.* **5**, 4713 [CrossRef Medline](#)
13. Yoshizumi, T., Imamura, H., Taku, T., Kuroki, T., Kawaguchi, A., Ishikawa, K., Nakada, K., and Koshiba, T. (2017) RLR-mediated antiviral innate immunity requires oxidative phosphorylation activity. *Sci. Rep.* **7**, 5379 [CrossRef Medline](#)
14. Castanier, C., Garcin, D., Vazquez, A., and Arnoult, D. (2010) Mitochondrial dynamics regulate the RIG-I-like receptor antiviral pathway. *EMBO Rep.* **11**, 133–138 [CrossRef Medline](#)
15. Wan, S., Ashraf, U., Ye, J., Duan, X., Zohaib, A., Wang, W., Chen, Z., Zhu, B., Li, Y., Chen, H., and Cao, S. (2016) MicroRNA-22 negatively regulates poly(I:C)-triggered type I interferon and inflammatory cytokine production via targeting mitochondrial antiviral signaling protein (MAVS). *Oncotarget* **7**, 76667–76683 [CrossRef Medline](#)
16. Subramanyam, D., Lamouille, S., Judson, R. L., Liu, J. Y., Bucay, N., Derynck, R., and Blesch, R. (2011) Multiple targets of miR-302 and miR-372 promote reprogramming of human fibroblasts to induced pluripotent stem cells. *Nat. Biotechnol.* **29**, 443–448 [CrossRef Medline](#)
17. Lin, S. L., Chang, D. C., Lin, C. H., Ying, S. Y., Leu, D., and Wu, D. T. (2011) Regulation of somatic cell reprogramming through inducible mir-302 expression. *Nucleic Acids Res.* **39**, 1054–1065 [CrossRef Medline](#)
18. Agarwal, V., Bell, G. W., Nam, J. W., and Bartel, D. P. (2015) Predicting effective microRNA target sites in mammalian mRNAs. *Elife* **4**, e05005 [CrossRef Medline](#)
19. Whittemore, L. A., and Maniatis, T. (1990) Postinduction turnoff of β -interferon gene expression. *Mol. Cell. Biol.* **10**, 1329–1337 [CrossRef Medline](#)
20. Otera, H., Ishihara, N., and Mihara, K. (2013) New insights into the function and regulation of mitochondrial fission. *Biochim. Biophys. Acta* **1833**, 1256–1268 [CrossRef Medline](#)
21. Alto, N. M., Soderling, J., and Scott, J. D. (2002) Rab32 is an A-kinase anchoring protein and participates in mitochondrial dynamics. *J. Cell Biol.* **158**, 659–668 [CrossRef Medline](#)
22. Bui, M., Gilady, S. Y., Fitzsimmons, R. E., Benson, M. D., Lynes, E. M., Gesson, K., Alto, N. M., Strack, S., Scott, J. D., and Simmen, T. (2010)

- Rab32 modulates apoptosis onset and mitochondria-associated membrane (MAM) properties. *J. Biol. Chem.* **285**, 31590–31602 [CrossRef Medline](#)
23. Cribbs, J. T., and Strack, S. (2007) Reversible phosphorylation of Drp1 by cyclic AMP-dependent protein kinase and calcineurin regulates mitochondrial fission and cell death. *EMBO Rep.* **8**, 939–944 [CrossRef Medline](#)
 24. Chang, C. R., and Blackstone, C. (2007) Cyclic AMP-dependent protein kinase phosphorylation of Drp1 regulates its GTPase activity and mitochondrial morphology. *J. Biol. Chem.* **282**, 21583–21587 [CrossRef Medline](#)
 25. Losón, O. C., Song, Z., Chen, H., and Chan, D. C. (2013) Fis1, Mff, MiD49, and MiD51 mediate Drp1 recruitment in mitochondrial fission. *Mol. Biol. Cell* **24**, 659–667 [CrossRef Medline](#)
 26. Palmieri, L., Pardo, B., Lasorsa, F. M., del Arco, A., Kobayashi, K., Iijima, M., Runswick, M. J., Walker, J. E., Saheki, T., Satrustegui, J., and Palmieri, F. (2001) Citrin and aralar1 are Ca²⁺-stimulated aspartate/glutamate transporters in mitochondria. *EMBO J.* **20**, 5060–5069 [CrossRef Medline](#)
 27. Thangaratnarajah, C., Ruprecht, J. J., and Kunji, E. R. (2014) Calcium-induced conformational changes of the regulatory domain of human mitochondrial aspartate/glutamate carriers. *Nat. Commun.* **5**, 5491 [CrossRef Medline](#)
 28. Yoshinaka, T., Kosako, H., Yoshizumi, T., Furukawa, R., Hirano, Y., Kuge, O., Tamada, T., and Koshihata, T. (2019) Structural basis of mitochondrial scaffolds by prohibitin complexes: insight into a role of the coiled-coil region. *iScience* **19**, 1065–1078 [CrossRef Medline](#)
 29. Hou, F., Sun, L., Zheng, H., Skaug, B., Jiang, Q.-X., and Chen, Z. J. (2011) MAVS forms functional prion-like aggregates to activate and propagate antiviral innate immune response. *Cell* **146**, 448–461 [CrossRef Medline](#)
 30. Sasaki, O., Yoshizumi, T., Kuboyama, M., Ishihara, T., Suzuki, E., Kawabata, S., and Koshihata, T. (2013) A structural perspective of the MAVS-regulatory mechanism on the mitochondrial outer membrane using bioluminescence resonance energy transfer. *Biochim. Biophys. Acta* **1833**, 1017–1027 [CrossRef Medline](#)
 31. Amoedo, N. D., Punzi, G., Obre, E., Lacombe, D., De Grassi, A., Pierri, C. L., and Rossignol, R. (2016) AGC1/2, the mitochondrial aspartate-glutamate carriers. *Biochim. Biophys. Acta* **1863**, 2394–2412 [CrossRef Medline](#)
 32. Alkan, H. F., Walter, K. E., Luengo, A., Madreiter-Sokolowski, C. T., Stryeck, S., Lau, A. N., Al-Zoughbi, W., Lewis, C. A., Thomas, C. J., Hoefler, G., Graier, W. F., Madl, T., Vander Heiden, M. G., and Bogner-Strauss, J. G. (2018) Cytosolic aspartate availability determines cell survival when glutamine is limiting. *Cell Metab.* **28**, 706–720.e6 [CrossRef Medline](#)
 33. Patterson, J. N., Cousteils, K., Lou, J. W., Manning Fox, J. E., MacDonald, P. E., and Joseph, J. W. (2014) Mitochondrial metabolism of pyruvate is essential for regulating glucose-stimulated insulin secretion. *J. Biol. Chem.* **289**, 13335–13346 [CrossRef Medline](#)
 34. Vacanti, N. M., Divakaruni, A. S., Green, C. R., Parker, S. J., Henry, R. R., Ciaraldi, T. P., Murphy, A. N., and Metallo, C. M. (2014) Regulation of substrate utilization by the mitochondrial pyruvate carrier. *Mol. Cell* **56**, 425–435 [CrossRef Medline](#)
 35. Chan, Y. K., and Gack, M. U. (2015) RIG-I-like receptor regulation in virus infection and immunity. *Curr. Opin. Virol.* **12**, 7–14 [CrossRef Medline](#)
 36. Forster, S. C., Tate, M. D., and Hertzog, P. J. (2015) MicroRNA as type I interferon-regulated transcripts and modulators of the innate immune response. *Front. Immunol.* **6**, 334 [CrossRef Medline](#)
 37. Barroso-delJesus, A., Romero-López, C., Lucena-Aguilar, G., Melen, G. J., Sanchez, L., Ligeró, G., Berzal-Herranz, A., and Menendez, P. (2008) Embryonic stem cell-specific miR302–367 cluster: human gene structure and functional characterization of its core promoter. *Mol. Cell. Biol.* **28**, 6609–6619 [CrossRef Medline](#)
 38. Chen, X., Zhou, L., Peng, N., Yu, H., Li, M., Cao, Z., Lin, Y., Wang, X., Li, Q., Wang, J., She, Y., Zhu, C., Lu, M., Zhu, Y., and Liu, S. (2017) MicroRNA-302a suppresses influenza A virus-stimulated interferon regulatory factor-5 expression and cytokine storm induction. *J. Biol. Chem.* **292**, 21291–21303 [CrossRef Medline](#)
 39. Yasukawa, K., Oshiumi, H., Takeda, M., Ishihara, N., Yanagi, Y., Seya, T., Kawabata, S., and Koshihata, T. (2009) Mitofusin 2 inhibits mitochondrial antiviral signaling. *Sci. Signal.* **2**, ra47 [CrossRef Medline](#)
 40. Bolstad, B. M., Irizarry, R. A., Astrand, M., and Speed, T. P. (2003) A comparison of normalization methods for high density oligonucleotide array data based on variance and bias. *Bioinformatics* **19**, 185–193 [CrossRef Medline](#)
 41. Gentleman, R. C., Carey, V. J., Bates, D. M., Bolstad, B., Dettling, M., Dudoit, S., Ellis, B., Gautier, L., Ge, Y., Gentry, J., Hornik, K., Hothorn, T., Huber, W., Iacus, S., Irizarry, R., et al. (2004) Bioconductor: open software development for computational biology and bioinformatics. *Genome Biol.* **5**, R80 [CrossRef Medline](#)
 42. Quackenbush, J. (2002) Microarray data normalization and transformation. *Nat. Genet.* **32**, 496–501 [CrossRef Medline](#)
 43. Yaku, K., Okabe, K., and Nakagawa, T. (2018) Simultaneous measurement of NAD metabolome in aged mice tissue using liquid chromatography tandem-mass spectrometry (LC/MS/MS). *Biomed. Chromatogr.* **32**, e4205 [CrossRef Medline](#)
 44. Yamamoto, M., Hikosaka, K., Mahmood, A., Tobe, K., Shojaku, H., Inohara, H., and Nakagawa, T. (2016) Nmnat3 is dispensable in mitochondrial NAD level maintenance *in vivo*. *PLoS ONE* **11**, e0147037 [CrossRef Medline](#)
 45. Saeed, A. I., Sharov, V., White, J., Li, J., Liang, W., Bhagabati, N., Braisted, J., Klapa, M., Currier, T., Thiagarajan, M., Sturn, A., Snuffin, M., Rezantsev, A., Popov, D., Ryltsov, A., et al. (2003) TM4: a free, open-source system for microarray data management and analysis. *BioTechniques* **34**, 374–378 [CrossRef Medline](#)